JOURNAL OF Materials CHEMISTRY

The near-surface defect structure of yttria-stabilised zirconia determined by measurement of the differential capacity

Johan E. ten Elshof,* Mark G. H. M. Hendriks, Henny J. M. Bouwmeester and Henk Verweij†

Laboratory of Inorganic Materials Science, MESA$^+$ Research Institute, University of Twente, P.O. Box 217, 7500 AE Enschede, the Netherlands.
E-mail: j.e.tenelshof@ct.utwente.nl

Received 26th January 2001, Accepted 7th June 2001
First published as an Advance Article on the web 7th August 2001

The space charge density at the surface of yttria-stabilised zirconia (YSZ) containing 2–10 mol% yttria was determined from differential capacity measurements of YSZ/gold interfaces at 750–850 K. The oxygen vacancy concentration in the sub-surface layer was determined as a function of temperature and bias potential by fitting the experimental data at positive bias potentials to predictions based on a Boltzmann-type expression. The vacancy concentration at the interface increases with decreasing bias potential, and reaches a temperature-dependent maximum value at negative bias potentials. The thermal activation parameter for this process is 0.27–0.46 eV. A thermodynamic model for the near-surface defect structure of YSZ is proposed, in which oxygen vacancies are assumed to be distributed randomly over a fraction of the total number of oxygen sub-lattice sites. The fraction of sites that is available for oxygen vacancy distribution increases with yttria content and temperature.

Introduction

Knowledge of the near-surface crystal defect structure of solid oxides is of importance for the understanding and further development of devices such as oxygen sensors,[1] oxygen separation membranes[2] and solid oxide fuel cells.[3] It is common to employ electron and ion spectroscopic techniques such as Auger spectroscopy (AES), X-ray photoelectron spectroscopy (XPS), transmission electron microscopy (TEM) and secondary ion mass spectroscopy (SIMS) in the investigation of oxide surfaces.[4] Indirect additional information may be obtained from transient experiments such as $^{18}O/^{16}O$ oxygen isotope exchange techniques.[5]

In the present paper a simple method to probe the near-surface space charge density of solid oxide electrolytes on the basis of differential capacity measurements at metal/electrolyte interfaces is proposed. The differential capacity measures changes in the near-surface concentrations of mobile charge carriers. The definition of the specific differential capacity C_{dif} is

$$C_{dif}(\varphi_b) = \left(\frac{d\sigma^M}{d\varphi_b}\right) \quad (1)$$

where σ^M is the surface charge density (C m^{-2}) on the metal, and φ_b is the applied bias potential. In literature the differential capacity of electrolytes is often referred to as the double-layer capacity. When the dielectric properties of the near-surface layer of the electrolyte is known, the space charge density in the oxide near the surface can be determined as a function of bias potential, temperature, and distance from the electrode.

The method is demonstrated here by differential capacity measurements on yttria-stabilised zirconia (YSZ)/gold interfaces, in which the majority of mobile charge carrier species are oxygen ions. Previous measurements on this system were explained in terms of a defect structure with randomly distributed, non-interacting oxygen vacancies.[6] The experimental data showed fair agreement with the trends predicted by this model. In the present paper an improved thermodynamic model for the near-surface defect structure of YSZ is developed, based on new experimental data.

The bulk defect structure of YSZ

At present more is known about the defect structure in the bulk of YSZ than about its near-surface defect structure. YSZ is formed by doping ZrO_2 with Y_2O_3 according to the overall reaction

$$Y_2O_3 \xrightarrow{ZrO_2} 2Y'_{Zr} + 3O^x_O + V^{\cdot\cdot}_O$$

using Kröger–Vink notation.[7]

From ionic conductivity measurements it is known that oxygen vacancies ($V^{\cdot\cdot}_O$) in the bulk of YSZ are (partially) immobilised at low temperatures.[8–11] Reported values for the association enthalpy of an oxygen vacancy vary from 0.28–0.36 eV for 2.8–12 mol% Y_2O_3-doped single crystals[12] to 0.49–0.57 eV for 10 mol% Y_2O_3-doped polycrystalline pellets[9] and 9.5–12 mol% Y_2O_3-doped single crystals.[13,14] A microscopic model for the ionic conductivity was developed by Solier *et al.*,[14,15] based on the assumption of randomly distributed non-interacting oxygen vacancies and partial vacancy trapping at lower temperatures. With this model it was determined that the fraction of mobile oxygen vacancies in 12 mol% Y_2O_3-doped YSZ single crystal reaches 50% at 1328 K.[14] It has been suggested that the oxygen vacancies are trapped by dopant ions with an effectively negative charge,[8,11,16,17] *i.e.*, defect interactions such as $V^{\cdot\cdot}_O + Y'_{Zr} = (V_O - Y_{Zr})$ and $V^{\cdot\cdot}_O + 2Y'_{Zr} = (Y_{Zr} - V_O - Y_{Zr})$ are assumed to occur. At dopant concentrations of 8 mol% Y_2O_3 or more, such defect interactions are thought to predominate. This assumption appears to be confirmed by results from a quasi-elastic light scattering study on polycrystalline YSZ samples containing 7–15 mol% Y_2O_3, which showed that the mobile charge carrier concentration decreases steadily over the entire

†Present address: Department of Materials Science and Engineering, Ohio State University, Columbus, Ohio, USA.

 DOI: 10.1039/b100923k

This journal is © The Royal Society of Chemistry 2001

composition interval.[18] However, it has been argued that Zr^{4+} is much more likely to be 7-fold coordinated by oxygen ions than Y^{3+}.[19]

Recently, an extensive high temperature (300–1800 K) neutron and X-ray diffraction study of YSZ containing 10–24 mol% Y_2O_3 was reported by Goff *et al.*[20] They found indications that the principal mobile defect consists of an isolated pair of oxygen vacancies located on opposite sides of a central cation. Taking those cations and anions surrounding the vacancies that undergo lattice relaxations into account, an $M_7O_{12}V_2$ (M = Zr,Y; V = oxygen vacancy) cluster was identified as the structural defect unit. The central cation is most likely Zr^{4+}.[20,21] Small static aggregates (correlation length ~5–15 Å) of clusters, consisting of close-packed $M_7O_{12}V_2$ units, were observed in compositions with 12 mol% Y_2O_3 or more. In addition to these two types of defective regions, a third type of region (size ~20 Å) with tetragonal distortion and very low oxygen vacancy concentration was observed. Using electron spin resonance, Orera *et al.*[22] found evidence for the same type of divacancy cluster, but also observed isolated $(V_O - Y_{Zr})^{\cdot}$ clusters.

Space charge density and differential capacity

Using the appropriate boundary conditions, the space charge density $\rho(x)$ (C m^{-3}) in an oxide at a distance x from a flat oxide/metal interface at $x = 0$ can be calculated from the Poisson equation in one-dimensional form

$$\left(\frac{d^2\varphi(x)}{dx^2}\right) = -\frac{4\pi\rho(x)}{\varepsilon}, \quad (2)$$

where ε is the dielectric constant of the oxide ($= \varepsilon_0\varepsilon_r$, with ε_0 the permittivity of vacuum, and ε_r the relative dielectric constant of the oxide). The space charge density expresses the net charge per unit volume and can be written in terms of a sum of (quasi-chemical) defect concentrations (vacancies, interstitial ions, *etc.*) only, *i.e.*,

$$\rho(x) = \sum_\alpha z_\alpha e c_\alpha(x), \quad (3)$$

with $c_\alpha(x)$ the concentration of defect α, z_α the formal charge, and e the electron charge. In the bulk,

$$\lim_{x\to\infty} \rho(x) = 0$$

The left hand side of eqn. (2) can be rewritten in terms of the electrical field strength $E(x) = -d\varphi(x)/dx$,[6] *i.e.*,

$$\left(\frac{d^2\varphi(x)}{dx^2}\right) = E(x)\left(\frac{dE(x)}{d\varphi(x)}\right). \quad (4)$$

The field strength $E(0)$ at the interface is related to σ^M on the metal *via* the dielectric constant: $\sigma^M = \varepsilon E(0)$. Upon inserting the latter equation into eqn. (4) and comparing the result with eqn. (2), an expression is obtained for the space charge density in the oxide at the interface $\rho(0)$:

$$\rho(0) = -\frac{\sigma^M}{4\pi\varepsilon}\left(\frac{d\sigma^M}{d\varphi(0)}\right). \quad (5)$$

With eqn. (1) and $\varphi(0) = \varphi_b$ it then follows that

$$\rho(0) = -\frac{\sigma^M C_{dif}(\varphi_b)}{4\pi\varepsilon}. \quad (6)$$

In three-point differential capacity measurements, φ_b is the applied bias potential. Hence, the space charge density at the interface of an oxide can be obtained from differential capacity measurements, if the dielectric constant at the interface is known.

Experimental

Polycrystalline yttria-stabilised zirconia powders containing 2, 3, 8 and 10 mol% yttria, respectively, were obtained commercially (Tosoh Corp., Tokyo, Japan). Their nominal purities are 99.3%, 99.3%, 98.5% and 99.8%, respectively. The main impurities as reported by the supplier are Al_2O_3, SiO_2, Fe_2O_3 and Na_2O, all with impurity levels below 0.5%. The powders with 2 and 3 mol% yttria have a tetragonal phase, while the compositions with 8 and 10 mol% yttria have a cubic phase.

The powders were pressed uniaxially at 75 MPa, followed by isostatic pressing at 400 MPa. The green compacts were sintered in air to densities higher than 99% of theoretical at 1500 °C for 6 h. The grain sizes varied from 2–8 μm for 2 mol% Y_2O_3-doped YSZ to 3–10 μm for 10 mol% Y_2O_3-doped YSZ.

For the differential capacity measurements the YSZ compacts were cut into discs (diameter 16.0 mm; thickness 4.0 mm) and polished with a 3 μm diamond emulsion. A circular notch was carved into the cylindrical side of the disc. Around the notch a platinum wire, serving as the reference electrode, was attached using platinum paste. One of the flat surfaces was painted with platinum paste and served as counter electrode. After firing at 1200 °C the Pt layer became porous, which is required to prevent polarisation at this electrode. The opposite flat surface was sputtered with a dense (ionically blocking) gold layer to serve as the working electrode. This type of cell with a reversible and an irreversible electrode is commonly referred to as the Hebb–Wagner cell, and is normally used for measuring the partial electronic conductivity in mixed ionic–electronic conductors. The sample was kept at constant temperature in an atmosphere that was flushed with nitrogen.

A bias potential was applied between the reference and working electrode (Potentiostat LB 75L, Bank Elektronik, Göttingen, Germany). Three-point electrical impedance spectroscopy measurements were performed at 10 mV rms using a frequency response analyser (Solartron Instruments 1250 FRA, Schlumberger Technologies Ltd., Farnborough, Hampshire, England) in the frequency range from 10 mHz to 60 kHz. The experimental impedance frequency dispersion curves were interpreted in terms of a constant phase element (CPE) and a resistance in parallel. The differential capacities were calculated from the CPE data.[23] Experiments were performed in the temperature range 748–848 K. At lower temperatures, the oxygen vacancies are rendered immobile. At temperatures above 873 K, the effect of slow sintering of the gold electrode made reliable measurements impossible.

Thermodynamic model

The thermodynamic model presented here is generally applicable to a system with well-defined defect species at low or intermediate concentrations. It will be used to develop defect models for YSZ and evaluate them on the basis of the experimental data.

The electrochemical potentials η_α of defects α present in the space charge region at a distance x from the interface, and in the bulk ($x\to\infty$), are related by $\eta_\alpha(x) = \eta_\alpha(x\to\infty)$ when the system is in equilibrium. The definition of the electrochemical potential of α reads

$$\eta_\alpha = \mu_\alpha^0 - Ts_\alpha + z_\alpha e\varphi, \quad (7)$$

where μ_α^0 is the standard chemical potential of α at temperature T, s_α is the partial configurational entropy, and φ is the local electrical potential. It is assumed that specific lattice relaxation effects and local Coulombic interactions between ions can be neglected. The above equilibrium can be rewritten as

$$\frac{1}{k_B}(s_\alpha(x) - s_\alpha(\infty)) = \frac{z_\alpha e\varphi(x)}{k_B T}. \quad (8)$$

Here k_B is the Boltzmann constant. Use was made of the fact

that

$$\lim_{x\to\infty}\varphi(x)=0$$

It is assumed that $s_\alpha(x)$ and $s_\alpha(\infty)$ have similar forms.

The configurational entropy S^{conf} of a crystalline system containing well-defined defect types β can be expressed in terms of the Boltzmann equation as

$$S^{\mathrm{conf}}=k_{\mathrm{B}}\sum_{\beta}\ln\Omega_\beta \tag{9}$$

The summation is over the respective numbers of permutations Ω_α of defects of type α present in the lattice. The partial molar entropy s_α can then be calculated from

$$s_\alpha=\left(\frac{\partial S^{\mathrm{conf}}}{\partial n_\alpha}\right)_{T,n_{\beta,\beta\neq\alpha}}, \tag{10}$$

with n_α and n_β the number of defects of types α and β, respectively.

To express the number of permutations Ω_α, an expression will be derived that bears close resemblance to part of a formalism originally introduced by Ling.[24,25] The formalism is generally applicable for well-defined "building block"-like defect types. In short, each defect present in an oxide lattice defines an "exclusion zone", a number of possible locations for other defects of the same or different type that can no longer be occupied due to the presence of the defect. Static and mobile defects of the same kind, *e.g.*, immobilised and mobile oxygen vacancies, can be treated as distinct types of defect species, either with or without a dynamic equilibrium acting between them. The exclusion zone is different for different types of defect species, and is characterised by the exclusion factor $\Lambda_{\alpha\beta}$, which indicates the number of lost permutations for a defect of type α due to the presence of a defect of type β.

The total number of possible sites for placement of n_α defects is approximately equal to $n_\alpha+N_{-\alpha}$, where $N_{-\alpha}$ is the potential number of sites that remains for placement of defects α after all defects have been distributed, *i.e.*,

$$N_{-\alpha}=M_\alpha^0-\sum_{\beta}\Lambda_{\alpha\beta}n_\beta$$

In the latter equation M_α^0 represents the number of permutations for placing an α-defect in a perfect, defect-free lattice. Then the number of permutations Ω_α for placement of n_α defects can be expressed by

$$\Omega_\alpha=(n_\alpha+N_{-\alpha})!/(n_\alpha!N_{-\alpha}!)$$

This results in

$$\Omega_\alpha=\frac{(M_\alpha^0-(\Lambda_{\alpha\alpha}-1)n_\alpha-\sum_{\beta\neq\alpha}\Lambda_{\alpha\beta}n_\beta)!}{n_\alpha!(M_\alpha^0-\sum_{\beta}\Lambda_{\alpha\beta}n_\beta)!}. \tag{11}$$

The above equation holds if the exclusion zones of neighbouring defects do not overlap. The value of M_α^0 is determined entirely by the symmetry of the crystal and the defect species under consideration. If the system consists of N unit cells, and with κ_α permutations for α per unit cell, it follows that $M_\alpha^0=\kappa_\alpha N$. In the case of zirconia the unit cell is Zr_4O_8. Hence, for simple oxygen vacancies $V_{\ddot{O}}$ (denoted with "V"), $\kappa_V=8$, while for linear divacancy pairs[20,22] $(V_O-M-V_O)^4$ (denoted with "D"), $\kappa_D=32$. Similarly, the number of defects can be expressed in the form $n_\alpha=x_\alpha\chi_\alpha N$, with x_α the molar fraction of defects, and χ_α the theoretically attainable defect concentration per unit cell. For isolated vacancies, $\chi_V=8$, while $\chi_D=4$ for divacancy pairs. The effects of an aggregate phase can be included in this model by subtracting the total volume it occupies from M_α^0, and distributing all mobile defects over the remaining configurational space.

Please note that in the present paper the $\Lambda_{\alpha\beta}$ values are treated as free fit parameters, which is different from the approach outlined in Ling's original formalism.[24,25] Moreover, in contrast to Ling, we include the exclusion factors $\Lambda_{\alpha\alpha}$,[26] while Coulombic interactions between defects are neglected. The latter is justified based on the results displayed in Fig. 6 of ref. 24. It is shown there that inclusion of Coulombic interactions does not lead to significantly different defect concentrations, as long as the effect of site exclusion is included.

Results and discussion

Due to pressure build-up of oxygen gas at the gold/YSZ interface at high (positive) potential, no differential capacity measurements were performed at bias potentials φ_b over +50 mV. In the low potential regime, measurements were performed down to bias potentials at which the data could no longer be interpreted in terms of a circuit consisting of a resistance and a CPE with power $n>0.85$ in parallel. Depending on composition and temperature, this lower limit was between –50 mV and –250 mV.

Fig. 1 shows the measured differential capacities of 8 mol% Y_2O_3-doped YSZ at different temperatures. The following discussion will be limited mainly to the analysis of these data. It should be stressed that similar trends were observed for the other compositions, and the analysis of those data is therefore the same as that discussed below.

Reported values for the bulk dielectric constant ε_r of YSZ at room temperature ($f>1$ kHz) are 39–41 for tetragonal (2–6 mol% Y_2O_3) zirconia[6,27] and 23–30 for cubic YSZ.[6,28–30] In the present experiments however, where only the near-surface layer is probed, the local dielectric constant may deviate strongly from its bulk value. It has in fact been shown by numerical simulation that the dielectric constant of the first few atomic layers near the surface of a dielectric material is smaller than its bulk value by up to more than an order of magnitude.[31] This permittivity-decreasing effect is entirely due to the presence of an interface and its effect on the ionic polarisability in the near-surface layers.

In the differential capacity experiments presented here it was observed that the absolute values of the differential capacity varied from one sample to the other by factors up to 3, but the exhibited trends were the same in all cases. It is well known that measurement of absolute double-layer capacities is very complicated.[32] However, it is reasonable to assume that the observed complex trends of the differential capacity with variation of φ_b and temperature can not be explained by the presence at the interface of non-ion conducting phases, such as Ca and Al compounds,[33,34] glassy silicates[35,36] and Y_2O_3.[37] We therefore attribute the observed trends to the near-surface defect structure of YSZ. Since the absolute value of C_{dif} is

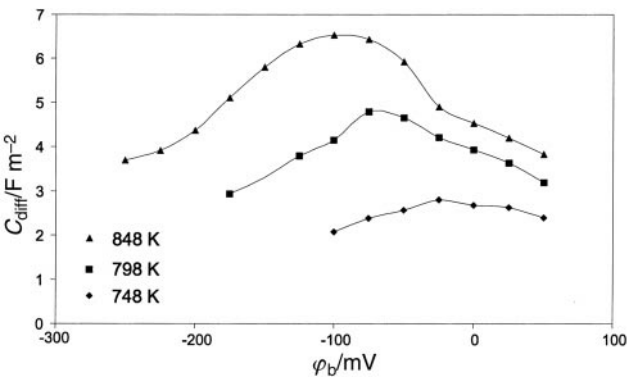

Fig. 1 Differential capacities of 8 mol% Y_2O_3-doped YSZ *vs.* bias potential.

affected by phenomena such as surface roughness[38] and segregated second phases present at the surface,[33–37] we will focus primarily on the formerly mentioned variation of the differential capacity with potential.

Therefore, the dielectric constant ε_r is treated as a fit parameter only, and its value is determined for each individual C_{dif}–φ_b isotherm. For the sake of simplicity, it is assumed that ε_r is independent of φ_b. This may be a simplification of the real situation. The oxygen vacancy concentration $[V_O^{\cdot\cdot}]$ per unit cell can be calculated using eqn. (3):

$$[V_O^{\cdot\cdot}] = \frac{\rho(0)v_0 + e[Y'_{Zr}]}{2e} \quad (12)$$

Here $[Y'_{Zr}]$ is the concentration of yttrium per unit cell. Based on reported lattice parameters $a = 5.145$–5.150 Å for $(Zr,Y)_4O_8$,[39] the unit cell volume v_0 was taken equal to 136.4 Å^3 in all calculations. The value of $\rho(0)$ can be calculated when a certain value for ε_r is assumed.

For the sake of illustration, Fig. 2 shows some cases constructed from the data shown in Fig. 1. The oxygen vacancy fraction x_V is defined as $x_V = [V_O^{\cdot\cdot}]/\chi_V$. If we consider that the electrolyte surfaces used in the experiments were polished prior to deposition of the gold layer, any segregated surface layers will have been removed. Furthermore, the experiments were conducted at temperatures far below those at which cation segregation becomes significant ($\sim$1300 K).[40,41] It may thus be assumed that the near-surface concentration $[Y'_{Zr}]$ in eqn. (12) is equal to the bulk concentration.

The theoretically attainable minimum and maximum values for the mole fraction of oxygen vacancies are indicated in Fig. 2 by dotted lines. It is immediately clear from this Figure that assigning values $\varepsilon_r < 10$ leads to physically impossible values for x_V. To find a more accurate estimate of ε_r, a Boltzmann-type expression is used below to fit the experimental curves.

Expressing defect concentrations using a Boltzmann-type expression is commonly applied for both ionic[42,43] and electronic[44] defects in space charge layers. Since site exclusion effects are neglected in this model, the molar defect fractions x_α follow simple exponential behaviour, *i.e.*,

$$x_\alpha = x_\alpha^0 \exp(-z_\alpha e\varphi/k_B T), \quad (13)$$

where x_α^0 is the α defect fraction at zero bias potential, and $\alpha = V$ (vacancy) or D (divacancy). This equation yields reliable predictions, provided that the overall defect concentrations in the system under consideration are low, and that the defect is sufficiently mobile to follow changes of potential (*i.e.*, defects are not irreversibly trapped, as for instance in ordered domains). Although it cannot explain the observed behaviour in YSZ over the entire potential range, the above expression may be utilised to fit the experimental data at high φ_b (≥ 0 V), where defect interactions and site exclusion effects are insignificant.

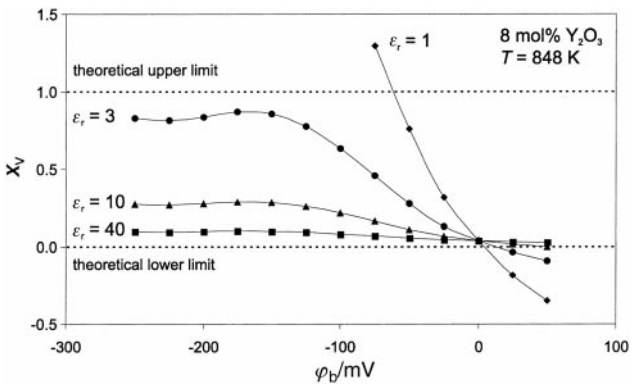

Fig. 2 Oxygen vacancy fractions in 8 mol% Y_2O_3-doped YSZ at 848 K as calculated from eqn. (6) for different values of the dielectric constant in the near-surface layer.

Optimised values for ε_r were determined by minimisation of the function Err, defined by

$$\mathrm{Err} = \sum_{\varphi_b \geq 0} \frac{(x_B(\varphi_b) - x_{exp}(\varphi_b))^2}{x_{exp}(\varphi_b)^2}. \quad (14)$$

Here x_{exp} is the defect mole fraction as calculated from the experimental data assuming a certain value for ε_r, and x_B is the defect mole fraction predicted from eqn. (13). For isolated oxygen vacancies, where $z_V = 2$ and $x_V^0 = x_V^{bulk}$, with x_V^{bulk} the fraction of oxygen vacancies in the bulk, the best fit for 8 mol% Y_2O_3-doped YSZ at 848 K shown in Fig. 2 was obtained with $\varepsilon_r = 14.0$. The experimental data, calculated for this value of ε_r, are shown in Fig. 3.

The same procedure was also applied to all other isothermal C_{dif} *vs.* φ_b curves. Although the absolute values of C_{dif} were not well reproducible, it was established that application of this procedure led to reproducible x_V *vs.* φ_b curves. The Err values are listed in Table 1. All fitted optimised values for ε_r were within the range 1–25.

The procedure was repeated for divacancy pairs[20] (D), with $z_D = 4$ and $x_D^0 = x_V^{bulk}$. The Err values were systematically larger than for single oxygen vacancies. This indicates that it is very unlikely that divacancy pairs are the majority charge carrier species at high bias potential.

It should be noted that a more complicated thermodynamic defect model we investigated, but not described in detail here, involved the mutual presence of isolated oxygen vacancies and

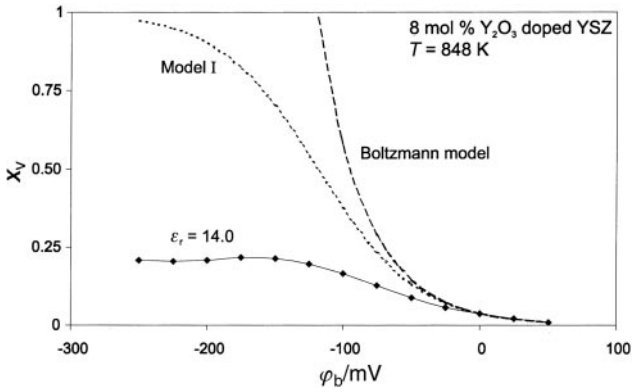

Fig. 3 Comparison of surface oxygen vacancy fractions of 8 mol% Y_2O_3-doped YSZ at 848 K as calculated from experimental data using eqn. (12) assuming $\varepsilon_r = 14.0$, and predicted values according to the Boltzmann-type expression (eqn. (13)) and Model I (random defect model).

Table 1 Values for the maximum near-surface mole fractions of defects at low bias potential, and error of fit (eqn. (14))

Composition Y_2O_3/mol%	T/K	Single vacancies		Divacancies	
		x_V^{max}	Err	x_D^{max}	Err
2	798	0.025	7.6×10^{-4}	(0.028)[a]	1.59
	848	0.031	0.016	0.034	0.18
3	798	0.047	7.8×10^{-3}	0.051	0.20
	848	0.061	2.4×10^{-3}	0.068	0.15
8	748	0.087	0.029	(0.12)[a]	1.26
	798	0.14	0.011	0.16	0.22
	848	0.21	0.015	0.26	0.20
10	748	0.15	0.057	0.17	0.35
	798	0.17	0.024	0.20	0.26
	848	0.33	0.014	0.40	0.20

[a]Best fit results in (physically impossible) defect concentrations below 0 at high bias potential.

Table 2 Description of models used in the text, and corresponding parameters as used in eqns. (7)–(11)

Model #	Description	Parameters
I	Non-interacting, randomly distributed oxygen vacancies (V).	$\kappa_V=8$, $\Lambda_{VV}=1$
II	Isolated oxygen vacancies (V); 100% mobile; maximum nonstoichiometry corresponds to that of M_7O_{12} phase.[48]	$\kappa_V=8$, $\Lambda_{VV}=7$
III	Isolated mobile (V) and trapped (T) oxygen vacancies. Trapping is associated with standard free energy change $\Delta g_r^0=\mu_V^0-\mu_T^0=\Delta h_r^0-T\Delta s_r^0$. IIIa: $\kappa_T=1$, $\Delta h_r^0=0.5$ eV, $\Delta s_r^0/k_B=4.81$; IIIb: $\kappa_T=1$, $\Delta h_r^0=0.5$ eV, $\Delta s_r^0/k_B=2.41$; IIIc: $\kappa_T=1$, $\Delta h_r^0=0.5$ eV, $\Delta s_r^0/k_B=0.12$; IIId: $\kappa_T=½$, $\Delta h_r^0=0.5$ eV, $\Delta s_r^0/k_B=0.12$.	$\kappa_V=8-\kappa_T$, $\Lambda_{VV}=1$, $\Lambda_{VT}=0$, $\Lambda_{TT}=1$, $\Lambda_{TV}=0$
IV	Volume fraction of mobile domain type increases with temperature. Configurational space is limited to conductive domain type.	$\kappa_V=8A\exp(-E/k_BT)$, $\Lambda_{VV}=1$

divacancy pairs, and the existence of a dynamic equilibrium between the two species. Two peaks were present in all C_{dif}–φ_b curves calculated using this model, one for each of the defect species present. The trends are qualitatively similar to the case of two mobile charges presented by Armstrong and Horrocks.[43] As the experimental data presented here show no indications of two peaks and can not be understood in terms of divacancies, models involving charge carriers other than single oxygen vacancies were not investigated further.

The simplest extension of the Bolzmann-type expression used above is to apply the condition of site exclusion.[6,8,45] The result is identical to a description in terms of the Ling formalism with parameters $\kappa_V=8$ and $\Lambda_{VV}=1$. This is Model I in Table 2, and this model was also used in our previous paper.[6] In Model I all vacancies are assumed to be randomly distributed over all possible oxygen lattice sites. A curve calculated with Model I is shown in Fig. 3. The curve does not deviate significantly from the predictions of the Boltzmann-type expression at high φ_b, but it can not explain the experimental behaviour at low potential.

The mole fractions of oxygen vacancies at the interface calculated using optimised ε_r-values and at different temperatures are shown in Fig. 4 for 8 mol% Y_2O_3-doped YSZ. The C_{dif}–φ_b isotherms behave identically at high φ_b, but deviate at lower values. Upon decreasing the bias potential further, a plateau is reached of which the level increases with temperature. The estimated height of the oxygen vacancy maximum is indicated by a dotted line for each temperature. The temperature dependency of the maximum can not be explained by the effect of site exclusion alone. Site exclusion is a steric effect, caused by the finite number of available lattice sites. It can be easily deduced from eqn. (11) that for a system with one type of defect, the limiting maximum number will be $n_\alpha \rightarrow M_\alpha^0/\Lambda_{\alpha\alpha}$, or, when expressed as a molar fraction of defects: $x_\alpha^{max} \rightarrow \kappa_\alpha^0/\chi_\alpha\Lambda_{\alpha\alpha}$.

Two examples of defect structures that have been proposed in the literature for the bulk of YSZ are Models II and III in Table 2. Fig. 5 shows C_{dif}–φ_b isotherms calculated with these models at 798 K. The experimental vacancy mole fractions of 8 mol% Y_2O_3-doped YSZ at 798 K, where $x_\alpha^{max} \approx 0.14$, are also shown.

In Model II it is assumed that all oxygen sites are available for distribution of defects ($\kappa_V=8$) and are energetically equivalent. All vacancies are assumed to be mobile. Each oxygen vacancy excludes its own lattice site from occupation by another vacancy, but also its 6 nearest neighbours ($\Lambda_{VV}=1+6=7$). Hence, $x_\alpha^{max}=1/7$ in Model II. This value corresponds with the maximum attainable oxygen deficiency in the ordered M_7O_{12} (M = Zr,Y) microdomains suggested by Goff *et al.*[20] The same oxygen deficiency also occurs in $Y_4Zr_3O_{12}$,[46] the only single-phase compound in the yttria–zirconia solid solution range,[47] and it has also been observed in several other anion-defective fluorite structures.[48]

Model III is an illustration of a case where a fraction of the oxygen vacancies is trapped at isolated oxygen sites that are homogeneously dispersed throughout the zirconia phase.[14] The trapped defects, denoted with the letter 'T', are exchanged with mobile vacancies (V) *via* the exchange reaction $(V_O^{\cdot\cdot})_T=(V_O^{\cdot\cdot})_V$, so that in equilibrium, $\eta_T(x)=\eta_V(x)$. The latter equation can be rewritten to $(s_V(x)-s_T(x))/k_B=\Delta g_r^0/k_BT$. Here, $\Delta g_r^0=\Delta h_r^0-T\Delta s_r^0=\mu_V^0-\mu_T^0$, with Δh_r^0 and Δs_r^0 the standard enthalpy and entropy of the freeing process of the vacancy, respectively. The value $\Delta h_r^0=0.5$ eV was used in all examples of Fig. 5, as it is close to reported experimental data for the association enthalpy of single vacancies.[14] The trapped vacancies are distributed over $M_T^0=\kappa_T N$ sites, and the mobile vacancies over the remaining $M_V^0=(8-\kappa_T)N$ sites. Furthermore, it is assumed that simple site exclusion occurs, *i.e.*, $\Lambda_{VV}=\Lambda_{TT}=1$, from which it follows that $\Lambda_{TV}=\Lambda_{VT}=0$.

It is clear that neither of these two models can describe the experimental behaviour satisfactorily. The C_{dif}–φ_b isotherms corresponding to Model III exhibit two maxima, since there are two types of species, which is in conflict with the experimental behaviour. Irrespective of how the parameters are actually set

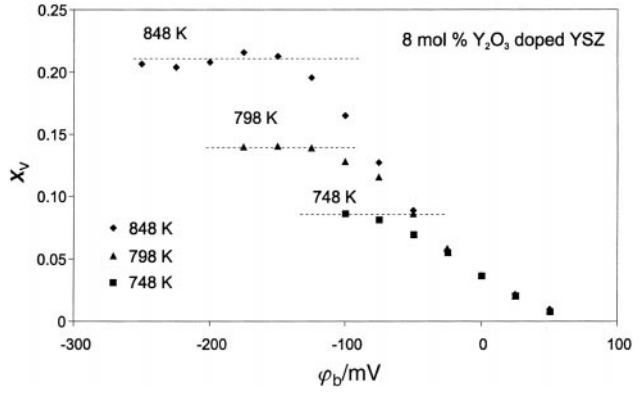

Fig. 4 Oxygen vacancy fractions in 8 mol% Y_2O_3-doped YSZ as a function of temperature and bias potential, calculated using optimised values for ε_r.

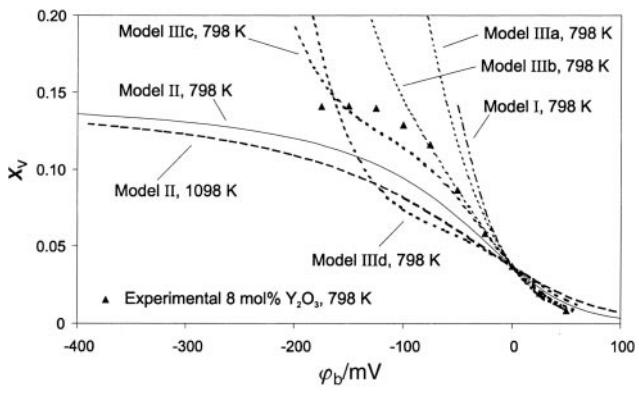

Fig. 5 Experimental oxygen vacancy fractions in 8 mol% Y_2O_3-doped YSZ at 798 K (using optimised ε_r), and curves calculated from Models I, II and III for 798 K and 1098 K.

in either model, no agreeable fit with the experimental data can be obtained. Moreover, in all models the plateaus at low bias potential (not shown in Fig. 5) are independent of temperature, which is in conflict with the experimental data.

To analyse the temperature dependency of the plateau region in more detail, the maximum attainable vacancy mole fraction x_V^{max} was fitted to an Arrhenius-type equation

$$x_V^{max}(T) = A \exp(-E/k_B T), \quad (15)$$

where E is an activation energy or enthalpy-like parameter, and A the pre-exponential factor. See Fig. 6 for the resulting Arrhenius-type plots. The values for E and A for different YSZ compositions are listed in Table 3 and shown in Fig. 7. The x_V^{max} values of 2 and 3 mol% Y_2O_3-doped YSZ used for fitting to eqn. (15) are estimated from the experimental trends, since the plateaus could not be observed directly in the data in these cases. Both E and ln A can be seen to increase with yttria content within experimental error.

Within the general framework of the thermodynamic model outlined in the previous section, the temperature dependency can be accounted for by making the parameters κ_α and/or $\Lambda_{\alpha\beta}$ temperature-dependent. Although it is possible that $\Lambda_{\alpha\beta}$ is influenced by temperature to some extent, from a physical point of view it is highly improbable that site exclusion would be the main cause of vacancy immobilisation at low temperatures. It therefore appears more likely that κ_α is temperature dependent.

A quantitative physical explanation for the observed temperature dependency can be given if it is assumed that the oxygen vacancies are distributed randomly over a fraction of the oxygen sub-lattice. The remaining part of the oxygen sub-lattice is non-conductive and inaccessible to oxygen vacancies. When the total number of oxygen sites available for oxygen vacancy distribution increases with temperature, the experimentally determined value of x_V^{max} can express the fraction of the total volume that is accessible to vacancy distribution. In terms of the thermodynamic formalism, this implies that $\kappa_V = 8x_V^{max}$, if Λ_{VV} is set to 1. This model will be referred to as Model IV. The total configurational space available for oxygen vacancy distribution is less than in Models I–III. Curves calculated using Model IV are shown in Figs. 8–10 for the investigated compositions. The qualitative

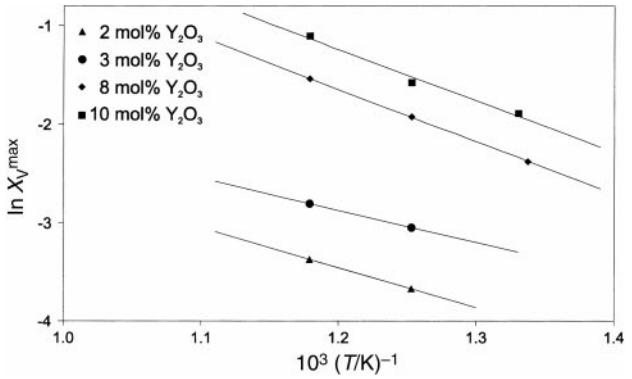

Fig. 6 Arrhenius-type representation of the oxygen vacancy fractions in the plateau regions listed in Table 3.

Table 3 Fitted parameters A and E from eqn. (15) and T_{crit} (eqn. (18)) for several YSZ compositions

Composition/mol% Y_2O_3	ln A	E/eV	T_{crit}/K
2	0.58 ± 2.03	0.29 ± 0.15	6.5×10^2
3	0.76 ± 1.17	0.27 ± 0.09	6.3×10^2
8	4.81 ± 0.24	0.46 ± 0.02	6.6×10^2
10	5.76 ± 1.67	0.45 ± 0.11	5.9×10^2

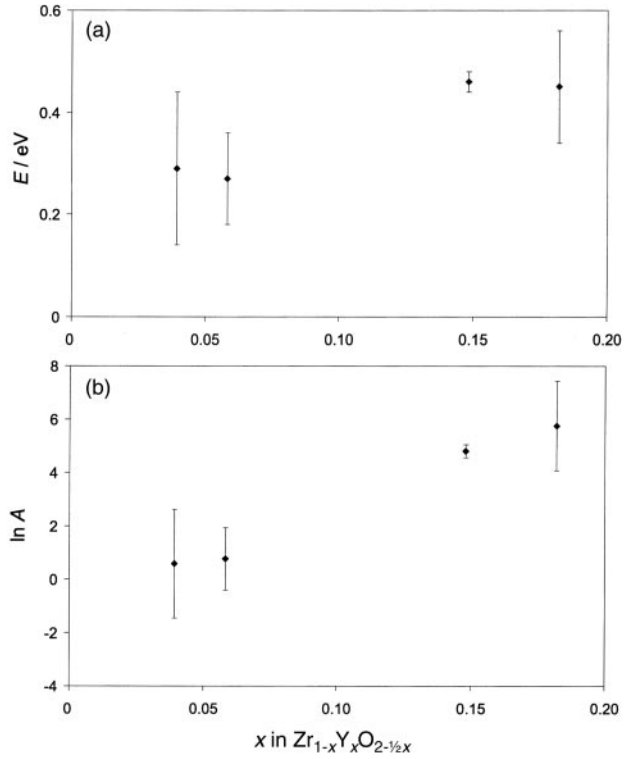

Fig. 7 Fitted parameters (a) E (eV) and (b) ln A from eqn. (15) *vs.* yttrium content x.

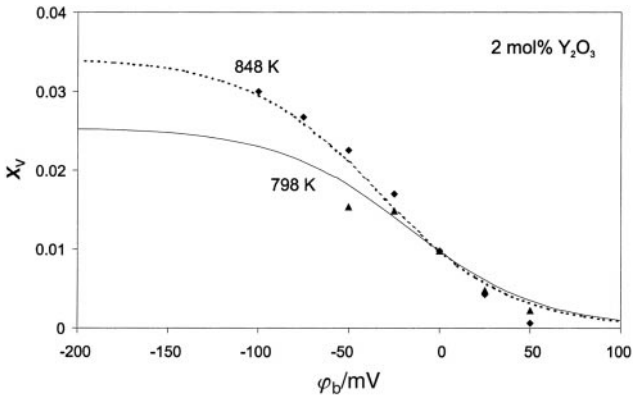

Fig. 8 Experimental oxygen vacancy fractions in 2 mol% Y_2O_3-doped YSZ, and predicted curves calculated from Model IV for the same set of temperatures.

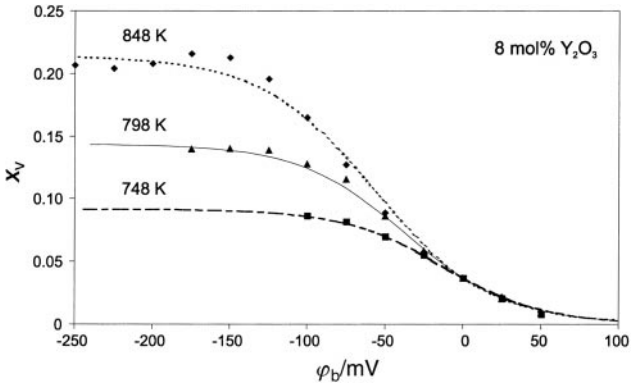

Fig. 9 Experimental oxygen vacancy fractions in 8 mol% Y_2O_3-doped YSZ, and predicted curves calculated from Model IV for the same set of temperatures.

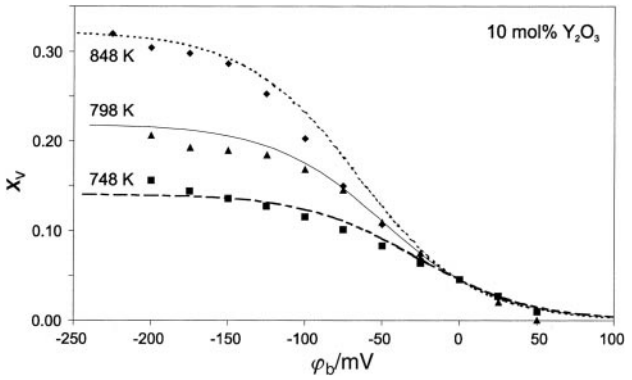

Fig. 10 Experimental oxygen vacancy fractions in 10 mol% Y_2O_3-doped YSZ, and predicted curves calculated from Model IV for the same set of temperatures.

agreement between the theoretical and experimental curves is good, the quantitative agreement is reasonable to good.

From eqns. (10) and (11), the configurational entropy of single oxygen vacancies can be calculated explicitly:

$$s_V = -k_B \ln\left(\frac{x_V}{x_V^{max}(T) - x_V}\right). \quad (16)$$

It then follows from eqn. (8) that

$$x_V = \frac{x_V^{max}(T) x_V^{bulk} \exp(-2e\varphi/k_B T)}{x_V^{max}(T) + x_V^{bulk}(\exp(-2e\varphi/k_B T) - 1)}. \quad (17)$$

The lower limiting temperature T_{crit} where Model IV is still valid can be estimated from the condition $x_V^{bulk} = x_V^{max}$ that follows for the bulk from eqn. (16). This yields

$$T_{crit} = \frac{E}{k_B ln(A/x_V^{bulk})}. \quad (18)$$

Estimated values of T_{crit} are listed in Table 3. The data are in good agreement with the supposition of Léon *et al.*[13] that below $\sim$673 K the ionic conductivity of oxygen is due to collective movement.

The supposed conductive and non-conductive domains in the near-surface layer of YSZ may be related to the observed tetragonal and cubic phases that coexist in the bulk of YSZ in the temperature range in which the measurements were performed.[49] It is also well possible that the different domains can not be distinguished directly by diffraction measurements, as their correlation lengths may be too small. The existence and behaviour of these types of domains can be understood by making an analogy with the commonly known melting trajectories that are found in mixtures of (related) substances. In a similar way, a region in YSZ may become penetrable for mobile oxygen vacancies at higher or lower temperature, depending on the details of the local environment on the atomic scale, *e.g.*, the crystal structure and local concentration of yttrium ions. This kind of behaviour can exhibit the type of temperature dependency that is seen in the experiments.

Conclusions

It was demonstrated that differential capacity measurements on oxidic electrolyte/metal interfaces can be helpful in the elucidation of the near-surface defect structure of the electrolyte phase. Upon measuring the variation of differential capacity with bias potential, the oxygen vacancy mole fractions in the surface layer of YSZ could be determined as a function of bias potential in the temperature range 748–848 K.

The relative dielectric constant, of which the near-surface value differed for each sample, was determined for each C_{dif}–φ_b isotherm by fitting the experimental data to theoretical curves predicted by the Boltzmann-type expression at high bias potential. The assumption was made that the near-surface dielectric constant is independent of the oxygen vacancy concentration.

On the basis of a general thermodynamic formalism and the experimental data, a model to describe the surface defect structure of YSZ was developed. Models that comply with defect structures already proposed in the literature for the bulk of YSZ were evaluated, but were found to provide an inadequate description of the defect structure at the surface of YSZ.

The experimental behaviour could be understood by assuming that part of the surface layer of YSZ is inaccessible to oxygen vacancies. The vacancies are distributed randomly over the remaining lattice sites. The volume fraction of YSZ that is accessible for oxygen vacancy distribution increases with yttria content and temperature.

Acknowledgements

B. A. Boukamp is gratefully acknowledged for useful discussions and careful reading of the manuscript.

References

1 A. M. Azad, S. A. Akhbar, S. G. Mhaisalkar, L. D. Birkefeld and K. S. Goto, *J. Electrochem. Soc.*, 1992, **139**, 3690.
2 H. J. M. Bouwmeester, in *CRC Handbook of Solid State Chemistry*, ed. P. J. Gellings and H. J. M. Bouwmeester, CRC Press, Boca Raton, FL, 1996, p. 481.
3 N. Q. Minh, *J. Am. Ceram. Soc.*, 1993, **76**, 563.
4 S. P. S. Badwal, J. Drennan and A. E. Hughes, in *Science of Ceramic Interfaces*, ed. J. Nowotny, Elsevier, Amsterdam, 1991, p. 227.
5 J. A. Kilner, in *Proc. 2nd Intl. Symp. on Ionic and mixed conducting oxides*, ed. T. A. Ramanarayanan, W. L. Worrell and H. L. Tuller, The Electrochemical Society, Pennington, NJ, 1994, p. 174.
6 M. G. H. M. Hendriks, J. E. ten Elshof, H. J. M. Bouwmeester and H. Verweij, *Solid State Ionics*, submitted.
7 F. A. Kröger, *The Chemistry of Imperfect Crystals*, North-Holland, Amsterdam, 1964.
8 R. E. W. Casselton, *Phys. Status Solidi A*, 1970, **2**, 571.
9 J. E. Bauerle and J. Hrizo, *J. Phys. Chem. Solids*, 1969, **30**, 565.
10 Y. Suzuki, T. Takahashi and N. Nagae, *Solid State Ionics*, 1981, **3**(4), 483.
11 A. I. Ioffe, D. S. Rutman and S. V. Karpachov, *Electrochim. Acta*, 1978, **23**, 141.
12 S. P. S. Badwal and M. V. Swain, *J. Mat. Sci. Lett.*, 1985, **4**, 487.
13 C. León, M. L. Lucía and J. Santamaría, *Phys. Rev. B*, 1997, **55**, 882.
14 J. D. Solier, I. Cachadiña and A. Dominguez-Rodriguez, *Phys. Rev. B*, 1993, **48**, 3704.
15 I. Cachadiña, J. D. Solier and A. Dominguez-Rodriguez, *Phys. Rev. B*, 1995, **52**, 10872.
16 J. A. Kilner and R. J. Brook, *Solid State Ionics*, 1982, **6**, 237.
17 A. Nakamura and J. B. Wagner Jr., *J. Electrochem. Soc.*, 1986, **133**, 1542.
18 T. Suemoto and M. Ishigame, *Solid State Ionics*, 1986, **21**, 225.
19 S.-M. Ho, *Mater. Sci. Eng.*, 1982, **54**, 23.
20 J. P. Goff, W. Hayes, S. Hull, M. T. Hutchings and K. N. Clausen, *Phys. Rev. B*, 1999, **59**, 14202.
21 H. G. Scott, *Acta Crystallogr., Sect B*, 1977, **33**, 281.
22 V. M. Orera, R. I. Merino, Y. Chen, R. Cases and P. J. Alonso, *Phys. Rev. B*, 1990, **42**, 9782.
23 B. A. Boukamp, *Equivalent Circuit* software, University of Twente, Enschede, the Netherlands, 2nd edn., 1989.
24 S. Ling, *Phys. Rev. B*, 1994, **49**, 864.
25 S. Ling, *J. Phys. Chem. Solids*, 1994, **55**, 1445.
26 Eqn. (17) in ref. 24 can be rewritten to $\Omega_\alpha = (M_\alpha^0 - \sum_{\beta \neq \alpha} \Lambda_{\alpha\beta} n_\beta)!/n_\alpha!(M_\alpha^0 - n_\alpha - \sum_{\beta \neq \alpha} \Lambda_{\alpha\beta} n_\beta)!$ Hence, no explicit use is made of the exclusion factor $\Lambda_{\alpha\alpha}$.
27 D. P. Thompson, A. M. Dickens and J. S. Thorp, *J. Mater. Sci.*, 1992, **27**, 2267.
28 M. A. Subramanian and R. D. Shannon, *Mater. Res. Bull.*, 1989, **24**, 1477.

29 F. E. G. Henn, R. M. Buchanan, N. Jiang and D. A. Stevenson, *Appl. Phys. A*, 1995, **60**, 515.
30 G. A. Samara, *J. Appl. Phys.*, 1990, **68**, 4214.
31 K. Natori, D. Otani and N. Sano, *Appl. Phys. Lett.*, 1998, **73**, 632.
32 R. D. Armstrong and R. Mason, *J. Electroanal. Chem.*, 1973, **41**, 231.
33 J. Nowotny, in *Science of Ceramic Interfaces*, ed. J. Nowotny, Elsevier, Amsterdam, 1991, p. 69.
34 J. Nowotny, M. Sloma and W. Weppner, *Solid State Ionics*, 1988, **28–30**, 1445.
35 B. V. Narashima Rao and T. P. Schreiber, *J. Am. Ceram. Soc.*, 1982, **65**, C44.
36 R. Chaim, M. Rühle and A. H. Heuer, *J. Am. Ceram. Soc.*, 1985, **68**, 427.
37 F. T. Ciacchi, K. M. Crane and S. P. S. Badwal, *Solid State Ionics*, 1994, **73**, 69.
38 L. I. Daikhin, A. A. Kornyshev and M. Urbakh, *J. Chem. Phys.*, 1998, **108**, 1715.
39 D. W. Strickler and W. G. Carlson, *J. Am. Ceram. Soc.*, 1964, **47**, 122.
40 A. J. A. Winnubst, P. J. M. Kroot and A. J. Burggraaf, *J. Phys. Chem. Solids*, 1983, **44**, 955.
41 G. S. A. M. Theunissen, A. J. A. Winnubst and A. J. Burggraaf, *J. Mater. Sci.*, 1992, **27**, 5057.
42 J. Maier, *Prog. Solid State Chem.*, 1995, **23**, 171.
43 R. D. Armstrong and B. R. Horrocks, *Solid State Ionics*, 1997, **94**, 181.
44 A. Many, Y. Goldstein and N. B. Grover, in *Semiconductor Surfaces*, North Holland, Amsterdam, 1971, p. 128.
45 S. Jiang and J. B. Wagner Jr., *J. Phys. Chem. Solids*, 1995, **56**, 1101.
46 H. G. Scott, *Acta Crystallogr., Sect. B*, 1977, **33**, 281.
47 V. S. Stubican, R. C. Hink and S. P. Ray, *J. Am. Ceram. Soc.*, 1978, **61**, 17.
48 H. J. Rossel, *J. Solid State Chem.*, 1976, **19**, 103.
49 V. S. Stubican, R. C. Hink and S. P. Ray, *J. Am. Ceram. Soc.*, 1978, **61**, 17.